Journal of Innovative Optical Health Sciences
Vol. 3, No. 3 (2010) 177–181

DOI: 10.1142/S1793545810000988

A STUDY ON PENETRATION DEPTH OF POLARIZATION IMAGING

RAN LIAO[*], NAN ZENG[*], DONGZHI LI[*,†], TIANLIANG YUN[*,†],
YONGHONG HE[*] and HUI MA[*,†,‡]

[*]*Laboratory of Optical Imaging and Sensing*
Graduate School at Shenzhen, Tsinghua University
Shenzhen 518055, China

[†]*Key Laboratory for Molecular and Nanosciences of Education Ministry*
Department of Physics, Tsinghua University
Beijing 100084, China
[‡]*mahui@tsinghua.edu.cn*

Optical clearing improves the penetration depth of optical measurements in turbid tissues. Polarization imaging has been demonstrated as a potentially promising tool for detecting cancers in superficial tissues, but its limited depth of detection is a major obstacle to the effective application in clinical diagnosis. In the present paper, detection depths of two polarization imaging methods, i.e., rotating linear polarization imaging (RLPI) and degree of polarization imaging (DOPI), are examined quantitatively using both experiments and Monte Carlo simulations. The results show that the contrast curves of RLPI and DOPI are different. The characteristic depth of DOPI scales with transport mean free path length, and that of RLPI increases slightly with g. Both characteristic depths of RLPI and DOPI are on the order of transport mean free path length and the former is almost twice as large as the latter. It is expected that they should have different response to optical clearing process in tissues.

Keywords: Polarization imaging; penetration depth; optical scattering.

1. Introduction

Polarization imaging has been applied to turbid tissues.[1–4] Since multiple scattering depolarizes the incident polarized light, penetration depth of polarization imaging based on differential polarization measurements is limited to the superficial layers of tissues. Optical clearing[5,6] can improve the penetration depth of optical measurements[7] and help clinical applications of polarization imaging.

There have been limited attempts to study the penetration depth of polarization imaging. Jacques *et al.* applied degree of polarization imaging (DOPI) to the skin pathology and showed that its imaging depth was less than 300 microns.[2,8] Liu *et al.* investigated the depth selective capability of polarization gating for tissue characterization.[9] Using Monte Carlo simulations and isotropic tissue phantom, they concluded that the depth of polarization imaging is on the order of the mean free path length. Using experiments and Monte Carlo simulations, Yao *et al.* have investigated the contrast mechanism of DOPI for three types of isotropic targets, i.e., reflecting, absorption and scattering.[10] They also concluded that the depths of DOPI for all the targets are a few mean free path lengths.

Recently, we developed rotating linear polarization imaging (RLPI)[11] which provides a set of parameters to quantitatively characterize the optical properties of anisotropic media. We also carried out further studies to examine the scattering behaviors of polarized photons in anisotropic media using Monte Carlo simulation[12] and to apply RLPI to clinical diagnosis of abnormal skin.[13] In this article, we use bovine skeletal muscles buried in the suspension of polystyrene spheres as the sample, and examine the characteristic depth behavior of RLPI and DOPI. Results of both experiments and Monte Carlo simulations show that the depth of DOPI scales with transport mean free path length and that of RLPI approximately scales with it. The penetration depth of RLPI also increases slightly as the anisotropic factor g increases. Depths of these two methods are on the order of transport mean free path length, and RLPI penetrates twice as deep as DOPI. These results can help us to study how optical clearing impoves the depth of polarization imaging.

2. Methods

Figure 1 shows a diagram of the experimental setup for RLPI and DOPI. Light of wavelength 650 nm from a 1-W LED is collimated by a lens L1, propagates through a rotatable linear polarizer P1 and illuminates the sample at 25° to the normal of sample surface. Backscattered photons from the sample pass through the rotatable analyzer P2 and are collected by lens L2 and recorded by CCD. By rotating both P1 and P2, polarization angles for illumination θ_i and for detection θ_s are changed. For RLPI, we first record a series of intensity images $I(\theta_i, \theta_s)$ and $I(\theta_i, \theta_s + \pi/2)$, and then calculate at each pixel the linear differential polarization (LDP), $[\mathrm{LDP}(\theta_i, \theta_s) \equiv I(\theta_i, \theta_s) - I(\theta_i, \theta_s + \pi/2)]$. The LDPs are fitted to Eq. (1) using a nonlinear least squares method to obtain a set of new parameters A, B, C, φ_1, and φ_3.[14]

$$\mathrm{LDP}(\theta_i, \theta_s) = \frac{1}{2} I_{\mathrm{in}} * \sqrt{A\cos(4\theta_s - \varphi_1) + B} * \cos[2\theta_i - \varphi_2(\theta_s)] + \frac{1}{2} I_{\mathrm{in}} * C * \cos[2\theta_s - \varphi_3]. \quad (1)$$

Each of these parameters forms its own pixel image. They are independent of incident and detection polarization angles and are related to different structural or optical properties of the sample. It was found that a derived parameter $G \equiv A/B$, can quantitatively characterize the anisotropic properties of the sample.[14] During each RLPI experiment, we can also obtain DOP images using intensity images corresponding to θ_i and $\theta_s = \theta_i + \pi/2$:

$$\mathrm{DOP} = \frac{I(\theta_i, \theta_i) - I(\theta_i, \theta_i + \pi/2)}{I(\theta_i, \theta_i) + I(\theta_i, \theta_i + \pi/2)}. \quad (2)$$

Since DOP is sensitive to the orientation of the fiber in the sample[8,14] and the polarization angle of the incident light,[15] in the present paper, we take DOP images with the incident polarization angles parallel to the fibrous structure at the surface of the sample. In contrast, G is insensitive to the orientation of the fibers in the sample and independent of the polarization angle of the incident light.[14]

3. Monte Carlo Analysis

As shown in Fig. 2, a fibrous medium as a target ("medium 2") is buried in the isotropic medium ("medium 1") with changing depth z_d. Medium 1 is the suspension of the microspheres. The surface plane of the sample is perpendicular to the Z-axis and the incident-detection plane in Fig. 1 is parallel to X–Z plane. Both the fiber orientation in the

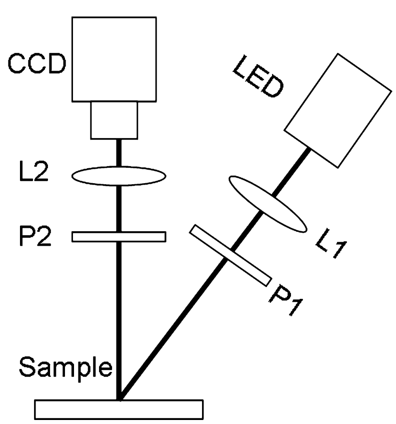

Fig. 1. Schematic diagram of the RLPI and DOPI experimental set-up.

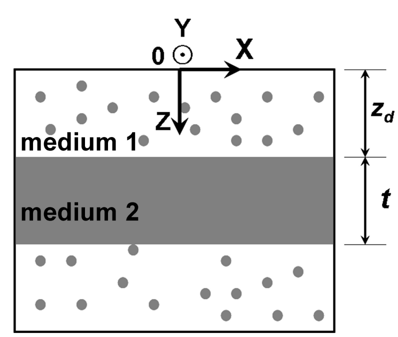

Fig. 2. The geometry of the sample under this study. The shadow part is the target.

anisotropic medium 2 and the 0° linear polarization angle of the incident light are parallel to X-axis, at which DOPs are obtained.

To quantitatively study the imaging depth of RLPI and DOPI for fibrous media, Monte Carlo simulation based on a sphere-cylinder scattering model[12,13] is used. We simulate the propagation of polarized photons in such sample and obtain G and DOP images. The diameters of the spherical and cylindrical scatterers are 1.5 μm and 2.0 μm respectively. Refractive indices of the spherical, cylindrical scatterers and the liquid are 1.59, 1.4, and 1.33 respectively. The scattering coefficients of the suspension and the fibrous medium are 30 cm^{-1} and 130 cm^{-1}. The cylinders are aligned along X-axis. The thickness of medium 2, t, is 2.0 cm and the depth of the target, z_d, changes from 0 to 9 mm.

We calculate contrasts of G and DOP to compare quantitatively the depth behavior of RLPI and DOPI:

$$\text{contrast} = \left|\frac{i_{\text{tar}} - i_{\text{bg}}}{i_{\text{tar}} + i_{\text{bg}}}\right|, \tag{3}$$

where i_{tar} and i_{bg} are the signal of the target (medium 2) and background (medium 1) respectively.[4,10] Figure 3 shows the contrast of G and DOP with different target depths z_d. One can find that contrasts for both G and DOP decrease as z_d increases, but the characteristic feature of the two curves are different. For z_d less than 9 mm, the contrast of G is higher than DOP.

From Fig. 3, we find that the contrast of DOP decreases continuously as z_d increases and that of G acts differently, which can be understood from the physics origin of them. DOP is the ratio of differential polarization of the total intensity backscattered from the sample; and G characterizes the anisotropic properties of the sample. According to Eq. (2), diffused photons are suppressed by the differential polarization in the numerator, but still included in the denominator. As z_d increases, the diffused photons gradually dominate the denominator,[8] and the ratio of the differential polarization of the total intensity decreases, that is, DOP drops. From Fig. 3, when z_d is about 2.8 mm, the contrast of DOP reduces to half of the value at $z_d = 0$. However, the contrast of G keeps at high level (>0.8) even when z_d is about 2.8 mm. It can be explained from the origin of G.[14] Even if the medium 2 is buried in medium 1 (2.8 mm deep), the entire sample is still anisotropic; and the order of the fiber alignment can be detected by RLPI and characterized by G. As z_d increases, the sample loses its anisotropic properties gradually, and the contrast of G drops to half of the value at $z_d = 0$ until z_d is about 6 mm. Based on the contrast curves of G and DOP, although they act differently, we can define the depth of G and DOP and study their properties quantitatively.

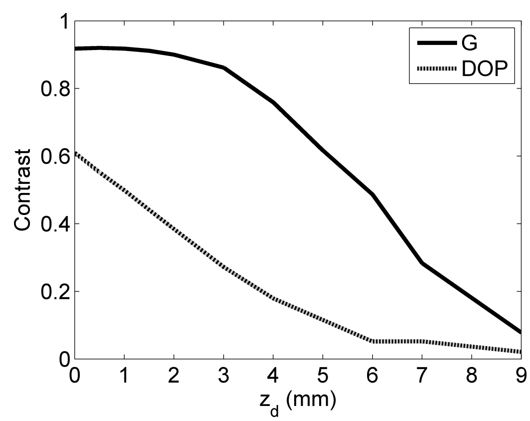

Fig. 3. Contrast of the simulation sample for DOP and G with different z_d.

To study the depth of RLPI and DOPI, we define the penetration depths of G and DOP as z_0. The FWHM of the characteristic curves in Fig. 3 shows that z_0 is 2.8 mm for DOP and 6.0 mm for G. We find that z_0 of DOP is about 8.4 times of mean free path ($mfp \equiv 1/\mu_s$) of medium 1, which is consistent with the finding by previous researchers.[9,10] Specially, z_0 of G is beyond the orders (18 times) of *mfp* and about 1.26 times of transport mean free path ($tmfp \equiv 1/[\mu_s(1-g)]$) length of medium 1.

To investigate the influence of the scattering properties of medium 1 on the penetration depths of DOP and G, simulations with different scattering coefficient μ_s and anisotropic factor g of medium 1 have been done and corresponding values of z_0 have been found and collected in Fig. 4.

For Fig. 4(a), $g = 0.93$ and μ_s increases from 20 to 60 cm^{-1}. We find that z_0 of DOP changes around the average 8.4 *mfp* in (a) and the deviation from the average value is within 3%. Similarly, z_0 of G changes around the average value 18 *mfp*, and the maximal deviation is less than 3%. We can find that both values of z_0 of DOP and G are linear with μ_s, and z_0 of DOP is about half of that of G.

For Figs. 4(b) and 4(c), $\mu_s = 30$ cm^{-1}, and g increases from 0.75 to 0.93. We find that z_0 of DOP normalized by *mfp* increases as g increases, and then tends to a stable value when it is normalized by *tmfp*. z_0 of G stays almost constant for

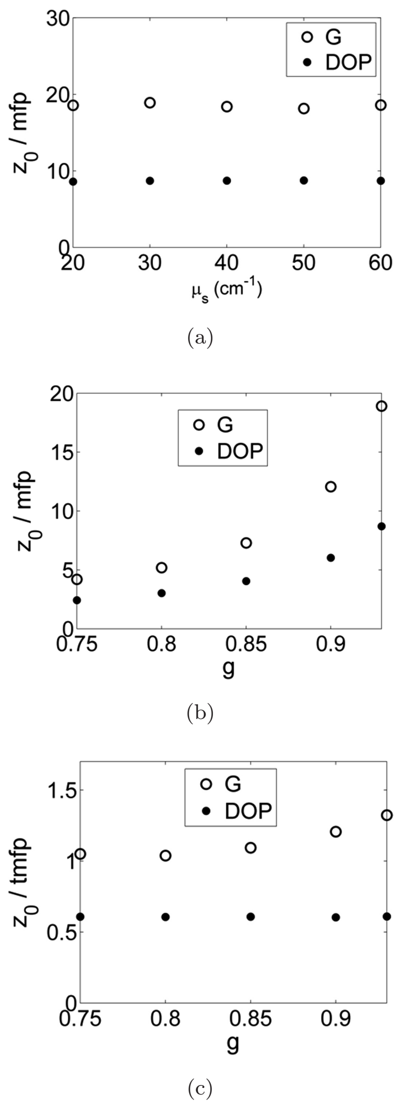

Fig. 4. z_0 of DOP and G vs. μ_s and g. For (a) and (b), z_0 is normalized by *mfp* of medium 1 and for (c), z_0 is normalized by *tmfp*. For (a), $g = 0.93$; and for (b)–(c), $\mu_s = 30\,\mathrm{cm}^{-1}$.

small g and increases as g becomes higher than 0.8 [see Fig. 4(c)]. In highly forward scattering region ($g > 0.9$), polarization is preserved for longer light paths.[9,16] However, z_0 of G is less than 1.3 *tmfp* even if $g = 0.93$. A close observation is made by fitting z_0 of G in Fig. 4(c) and we find that it can be expressed as a function of $g : a\exp[-b(1-g)] + c$, in which a, b, and c are variables. Mathematical calculation shows that all three variables are positive, and both a and c are less than 1.0, which means z_0 of G will be less than 2 *tmfp*. Then it can be concluded that z_0 of G is on the order of *tmfp* of medium 1.

From Fig. 4, we find that when the target is the optical anisotropic medium, z_0 of DOP can be normalized by *tmfp*. z_0 of G approximately scales with *tmfp* and although it slightly increases as g increases, it is still on the order of *tmfp*. Moreover, z_0 of DOP is less than half of that of G.

4. Experiment and Discussion

According to Fig. 2, a piece of 5 mm-thick bovine skeletal muscle (as "medium 2") is buried in the aqueous suspension of microspheres (as "medium 1") with depth z_d changing from 0 to 9 mm. The diameter of the microsphere in medium 1 is 1.5 μm, the refractive indices of the microsphere and liquid are 1.59 and 1.33 respectively. This corresponds to anisotropic factor $g = 0.93$ and the scattering coefficient of medium 1 is $30\,\mathrm{cm}^{-1}$. The isotropic medium 1 is contained in a glass container with an optical window towards the incident light. The fiber orientation in the medium 2 is along X-axis.

We calculate contrasts of DOP and G and present the results in Fig. 5. We can find that the contrast curves of DOP and G are similar to that in Fig. 3, and z_0 of DOP and G are respectively 0.60 *tmfp* and 1.28 *tmfp* of medium 1, which is consistent with the results obtained by Monte Carlo simulations.

Optical clearing increases the refractive index of the ambient substance around the scattering particles,[6] such as cells or organelles or the nucleus within a cell, and improves the refractive index matching, which reduces the scattering coefficient μ_s and increases the anisotropic factor g.[17] From the analysis in the above sections, we conclude that

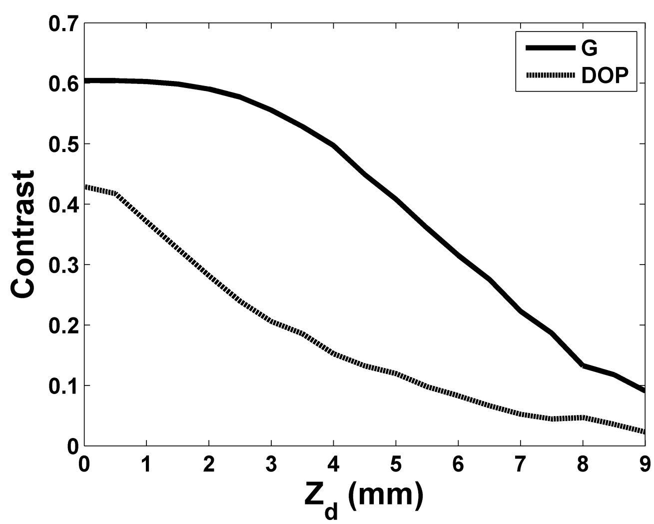

Fig. 5. The contrast of the experimental sample for DOP and G with different z_d.

the penetration depth z_0 of DOP and G will increase as the result of optical clearing. Penetration for the G images is almost twice as deep as that for DOP. The difference is even bigger with tissue clearing since phase matching increases g. It will be helpful to study optical clearing and polarization imaging, when they are applied to tissues at the same time. On the one hand, we can use the results in this paper to study quantitatively how optical clearing increases the penetration depth of RLPI and DOPI. On the other hand, RLPI and DOPI provide good tools to investigate the dynamics of optical clearing processes.

5. Conclusions

In this paper, penetration depths of RLPI and DOPI have been studied for the anisotropic media containing both cylindrical and spherical scatterers buried under an isotropic scattering medium. Results of both Monte Carlo simulations on a sphere-cylinder scattering model and experiments of bovine skeletal muscle buried in the aqueous suspension of polystyrene microspheres show that the depth of DOPI scales with transport mean free path length and that of RLPI approximately scales with it. The penetration depth of RLPI also increases slightly as the anisotropic factor g increases. Both the depths of RLPI and DOPI are on the order of transport mean free path length, and the former is almost twice as large as the latter. When optical clearing is applied, reduction of the scattering coefficient increases the penetration depths of both imaging methods, and increase of the anisotropic factor makes RLPI penetrate even deeper. Both methods can be used to study the optical clearing processes in tissues.

Acknowledgments

This work has been supported by National Natural Science Foundation of China (grants 60778044 and 10974114), and Ministry of Science and Technology (grant 2006CB70570).

References

1. S. G. Demos, R. R. Alfano, "Optical polarization imaging," *Appl. Opt.* **36**(1), 150–155 (1997).
2. S. L. Jacques, J. R. Roman, K. Lee, "Imaging skin pathology with polarized light," *J. Biomed. Opt.* **7**(3), 329–340 (2002).
3. S. P. Morgan, I. M. Stockford, "Surface-reflection elimination in polarization imaging of superficial tissue," *Opt. Lett.* **28**(2), 114–116 (2003).
4. H. R. Shao, Y. H. He, W. Li, H. Ma, "Polarization-degree imaging contrast in turbid media: A quantitative study," *Appl. Opt.* **45**(15), 4491–4496 (2006).
5. V. V. Bakutkin, I. L. Maksimova, T. N. Semyonova, V. V. Tuchin, I. L. Kon, "Controlling optical properties of sclera," *Proc. SPIE* **2393**, 137–141 (1995).
6. V. V. Tuchin, I. L. Maksimova, D. A. Zimnyakov, I. L. Kon, A. H. Mavlutov, A. A. Mishin, "Light propagation in tissues with controlled optical properties," *J. Biomed. Opt.* **2**(4), 401–407 (1997).
7. Y. H. He, R. K. Wang, "Dynamic optical clearing effect of tissue impregnated with hyerosmotic agents and studied with optical coherence tomography," *J. Biomed. Opt.* **9**(1), 200–206 (2004).
8. S. L. Jacques, J. R. Roman, K. Lee, "Imaging superficial tissues with polarized light," *Lasers Surg. Med.* **26**(2), 119–129 (2000).
9. Y. Liu, Y. L. Kim, X. Li, V. Backman, "Investigation of depth selectivity of polarization gating for tissue characterization," *Opt. Express* **13**(2), 601–611 (2005).
10. R. Nothdurft, G. Yao, "Expression of target optical properties in subsurface polarization-gating imaging," *Opt. Express* **13**(11), 4185–4195 (2005).
11. X. Y. Jiang, N. Zeng, Y. H. He, H. Ma, "Investigation of linear polarization difference imaging based on rotation of incident and backscattered polarization angles," *Pro. Biochem. Biophys.* **34**, 659 (2007).
12. T. Yun, N. Zeng, W. Li, D. Li, X. Jiang, H. Ma, "Monte Carlo simulation of polarized photon scattering in anisotropic media," *Opt. Express* **17**(19), 16590–16602 (2009).
13. N. Zeng, X. Jiang, Q. Gao, Y. He, H. Ma, "Linear polarization difference imaging and its potential applications," *Appl. Opt.* **48**(35), 6734–6739 (2009).
14. R. Liao, N. Zeng, X. Y. Jiang, D. Z. Li, T. Yun, Y. H. He, H. Ma, "A rotating linear polarization imaging technique for anisotropic tissues," *J. Biomed. Opt.* **15**(3), 2010, in press.
15. X. Wang, L. V. Wang, "Propagation of polarized light in birefringent turbid media: A Monte Carlo study," *J. Biomed. Opt.* **7**(3), 279–290 (2002).
16. V. Sanharan, M. J. Everett, D. J. Maitland, J. T. Walsh, "Comparison of polarized-light propagation in biological tissue and phantoms," *Opt. Lett.* **24**(15), 1044–1046 (1999).
17. C. F. Bohden, D. Huffman, "Electromagnetic theory," Chap. 2 in *Absorption and Scattering of Light by Small Particles*, pp. 44–56, Wiley, New York (1983).